Interfacial Adsorption of Antifreeze Proteins: A Neutron Reflection Study

Hai Xu,* Shiamalee Perumal,† Xiubo Zhao,† Ning Du,‡ Xiang-Yang Liu,‡ Zongchao Jia,§ and Jian R. Lu†
*Centre for Bioengineering and Biotechnology, China University of Petroleum (East China), Qingdao 266555, China; †Biological Physics, School of Physics and Astronomy, The University of Manchester, Manchester M13 9PL, United Kingdom; ‡Department of Physics, Faculty of Science, National University of Singapore, Singapore 117542; and §Department of Biochemistry, Queen's University, Kingston, Ontario, Canada K7L 3N6

ABSTRACT Interfacial adsorption from two antifreeze proteins (AFP) from ocean pout (*Macrozoarces americanus*, type III AFP, AFP III, or maAFP) and spruce budworm (*Choristoneura fumiferana*, isoform 501, or cfAFP) were studied by neutron reflection. Hydrophilic silicon oxide was used as model substrate to facilitate the solid/liquid interfacial measurement so that the structural features from AFP adsorption can be examined. All adsorbed layers from AFP III could be modeled into uniform layer distribution assuming that the protein molecules were adsorbed with their ice-binding surface in direct contact with the SiO_2 substrate. The layer thickness of 32 Å was consistent with the height of the molecule in its crystalline form. With the concentration decreasing from 2 mg/ml to 0.01 mg/ml, the volume fraction of the protein packed in the monolayer decreased steadily from 0.4 to 0.1, consistent with the concentration-dependent inhibition of ice growth observed over the range. In comparison, insect cfAFP showed stronger adsorption over the same concentration range. Below 0.1 mg/ml, uniform layers were formed. But above 1 mg/ml, the adsorbed layers were characterized by a dense middle layer and two outer diffuse layers, with a total thickness around 100 Å. The structural transition indicated the responsive changes of conformational orientation to increasing surface packing density. As the higher interfacial adsorption of cfAFP was strongly correlated with the greater thermal hysteresis of spruce budworm, our results indicated the important relation between protein adsorption and antifreeze activity.

INTRODUCTION

Over evolution pathways, different proteins and glycoproteins have been developed to suppress freezing points and protect organisms from freezing to death (1). Over the past few decades, four types of antifreeze proteins (AFP I–IV) and one type of glycoproteins (AFGP) have been identified from sea fish, in addition to those found in plants, insects, and bacteria (2–6). These AF(G)Ps are regarded as unusual because they can depress freezing points far greater than would be predicted from colligative properties alone. Extensive studies have suggested that they lower the freezing point by interacting with the ice surface and cause the nonequilibrium lowering of the freezing point below the melting point of the ice (thermal hysteresis). Despite excellent progress in the study of the interactions between antifreeze protein and ice, there is a lack of direct experimental evidence that would link antifreeze activity to the structural matching at the ice-protein interface as postulated from extensive x-ray diffraction and NMR studies. Although protein adsorption into ice is regarded as an important aspect of AFP research, there is little direct evidence of AFP adsorption at the ice/water interface due to experimental difficulty. The work reported below has taken the advantage of the recently developed neutron reflection to reveal the structural features of two AFP proteins, an AFP III from ocean pout (*Macrozoarces americanus*, maAFP) and an insect AFP from spruce budworm (*Choristoneura fumiferana*, cfAFP), with the latter having significantly greater antifreeze activity. Instead of attempting to undertake the measurement at the ice/water interface, the optically flat hydrophilic SiO_2 surface has been used as the model substrate.

AFPs isolated from fish have been most extensively studied. One of the early studies by Raymond and Davies (7) demonstrated the concentration-dependent thermal hysteresis from an AFGP. With sufficient AFP concentrations, fish antifreeze proteins offer protection against the freezing point of seawater down to −1.9°C. On land, winter temperatures could go below −30°C. Many species of insects such as *C. fumiferana* generate antifreeze proteins and small molecular weight chemicals such as glycerol to protect them from freezing (8,9). The antifreeze proteins are capable of depressing the freezing point of extracellular fluids and allowing larvae or insects to supercool.

Although each species produces mainly one or two types of antifreeze, they are usually composed of multiple active isoforms. In cfAFPs, at least seven different isoforms are known at the cDNA level (9). These different cDNAs encode proteins of two distinct sizes: ~9 kDa and 12 kDa, with the large one containing 30 or 31 amino acid insertions creating two additional 15 or 16 amino acid loops in the β-helix (cfAFP-501). This effectively increased the two-dimensional Thr array and the ice-binding surface. As a result, the larger AFP has greater thermal hysteresis than the 9 kDa AFP (cfAFP-337). Deletion of the 31-residue insertion resulted in the reduction of the thermal hysteresis activity similar to the smaller isoforms, indicating the strong correlation with the size of the Thr ice-binding surface. Although the longer

Submitted October 26, 2007, and accepted for publication December 11, 2007.

Address reprint requests to Jian R. Lu, Tel.: 44-161-306-3926; E-mail: j.lu@manchester.ac.uk.

Editor: Jill Trewhella.

0006-3495/08/06/4405/09 $2.00

doi: 10.1529/biophysj.107.124560

cfAFP-501 is only 66% identical to the shorter cfAFP-337, they both have a similar prism shape and carry the Thr-Xxx-Thr (Xxx stands for any amino acid) repeats on the flat ice-binding face. The larger ice-binding surface on cfAFP-501 is widely attributed to the greater inhibition in ice crystal growth. AFP proteins isolated from beetles and spruce budworms are usually far more effective on the molar basis than fish AFPs or antifreeze glycoproteins (1,10). The structures of the insect AFPs are unique, and unlike the fish AFPs they are β-helices with two rows of Thr residues down one side of the protein, making a good structural match to both prisms and basal planes.

For both fish and insects, thermal hysteresis increases with AFP concentrations (10). It has long been proposed that the adsorption of AFP molecules at the ice/water interface is facilitated by the structural complementarity between the ice-binding surface of the AFP and the binding site on the ice surface (1–6). High concentrations render greater surface adsorption, but how the exact adsorption occurs remains unknown due to the lack of experimental progress in the area. Given the vast structural differences between different AFPs, it seems that all of them tend to bind ice in a few categorized specificities. Adsorbed AFP molecules restrict ice from growing between the surface bound proteins within a local surface, making it energetically less favorable for water molecules to join the local lattice (11,12). Although this explanation is plausible, there is a lack of direct experimental evidence to link the local lattice matching to antifreeze activity. Furthermore, assuming the fundamental significance of the structural complementarity, it is yet unclear how different lattice structural matching affects the extent of thermal hysteresis and concentration dependence.

The different types of surface-specific binding from AF(G)Ps may also imply that these proteins must have similar physicochemical properties for surface and interfacial adsorption and that the binding surfaces are important only in a broad sense. This would mean that an important aspect of AF(G)P characterization is to assess their surface and interfacial adsorption properties and compare them with other proteins.

In this work, neutron reflection is used to probe the structural features of AFP protein layers adsorbed at the silicon oxide/water interface. SiO_2 has been widely used in neutron reflection as model surface to assess the adsorption characteristics of various other proteins (13–17). The proposed study enables a direct comparison between AFPs and other proteins from different biological sources. As the SiO_2 surface is covered with hydrated water molecules and is hydrophilic, it is a good compromise between ice surface mimicking and facilitation of the experimentation by neutron reflection. Our results from both AFPs have shown a remarkable correlation between the structure of the AFP layers and their different antifreeze activities. This work thus points to the significance of interfacial properties of AFPs to the ongoing effort toward understanding antifreeze mechanisms.

EXPERIMENTAL

Neutron reflection

Neutron reflection experiments were undertaken on a reflectometer SURF at Rutherford Appleton Laboratory near Oxford, UK. The experimental setup was similar to that described by Fragneto et al. (18). A stainless steel trough was clamped against the freshly cleaned surface of a silicon block and the sealing was achieved through the deployment of an O-ring surrounding the edges of the trough. The trough normally required ~2 ml solution to fill. The beam-illuminated area was typically ~8 cm × 3 cm and its exact size was defined by the horizontal and vertical slits placed before the sample setup.

The reflectometer used a white neutron beam with a wavelength ranging from 0.5 to 6 Å. Each reflection experiment was then carried out at three incidence angles of 0.35, 0.8, and 1.8°, and the resulting reflectivity profiles combined to cover a momentum transfer (κ) range between 0.01 and 0.5 $Å^{-1}$. For each reflectivity profile, a constant background was subtracted using the average reflectivity between 0.25 and 0.5 $Å^{-1}$. For a given solution, the time-dependent adsorption was monitored by repeating reflectivity measurements at different time intervals. It was found that for almost all the systems studied here, no time-dependent adsorption was detected some 10 min after the placement of the solutions in troughs. All neutron reflectivity profiles were measured after ~15 min solution equilibration.

AFPs

The first antifreeze studied was a type III protein produced from ocean pout (*M. americanus*) with Protein Data Bank code 1HG7. It has a total of 66 amino acids and the following sequence:

MNQASVVANQLIPINTALTLVMMRSEVVTPVGIPAEDIPRLVSMQVNR
AVPLGTTLMPDMVKGYAA.

It is composed of 16 different types of amino acids, the majority of which are hydrophobic. (V10I4L6A7M6 P6Q3K1R3D2E2YG3S3N4T5). With four cationic and four anionic amino acids, its isoelectric point is 7.1. The protein has no C groups for forming S=S bridges. The unit cell dimensions incorporating a single molecule are $a = 32$ Å, $b = 39$ Å, and $c = 45$ Å (3,19). Its globular structure is shown in Fig. 1. Its molecular weight is 7038 and the total scattering length density is 2.70×10^{-6} $Å^{-2}$ in D_2O.

The fish type III AFP was bought in lyophilized form from A/F Protein, St. John's, Newfoundland, Canada. It was extracted from the plasma of the *M. americanus* that were caught in spring and were then kept in holding tanks supplied with running, aerated seawater. As the cold water persisted, the fish produced antifreeze proteins. Blood was extracted from the fish and centrifuged to separate plasma from the cellular fraction. The plasma was put through a series of filtration steps to further refine the product and produce a clean solution for application to a chromatography column. The resulting column fractions were assayed for antifreeze activity. Fractions exhibiting

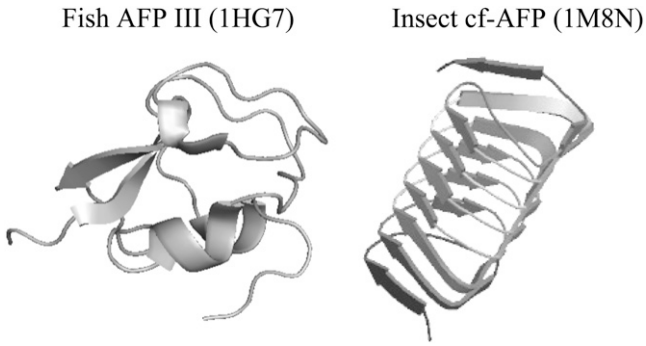

FIGURE 1 Molecular structure of AFP III (1HG7 from Antson et al. (3), *left*) and cf-AFP (1M8N from Leinala et al. (9), *right*).

thermal hysteresis were pooled and lyophilized to produce purified antifreeze protein. The purity of the lyophilized protein was checked from each batch using SDS-PAGE gel plating.

Circular dichroism (CD) spectra were measured using a Jasco (Tokyo, Japan) J-810 spectropolarimeter with a 1 mm cell path length. AFP III was dissolved in deionized water at a concentration of 0.2 mg/ml and the temperature was controlled at 22°C.

The second antifreeze protein studied was from *C. fumiferana* (cfAFP, also known as sbwAFP) (8,9,20). The insect produces a number of isoforms that are among the highest active antifreeze proteins reported so far. Isoform cfAFP, one 12.5 kDa isoform, has been characterized (namely 501 or cfAFP-501). It has a Protein Data Bank code of 1M8N and a total of 121 amino acids with the following sequence:

DGTCVNTNSQITANSQCVKSTATNCYIDNSQLVDTSICTRSQYSDANV
KKSVTTDCNIDKSQVYLTTCTGSQYNGIYIRSSTTTGTSISGPGCSISTC
TITRGVATPAAACKISGCSLSAM AA.

It is again composed of 16 different types of amino acids, the majority of which are also hydrophobic (V7I10L3A8M1P2Q6K5R3D6Y5G8C10S19-N8T20). With eight cationic amino acids and six anionic Ds, its isoelectric point is 7.8. Its number of amino acids is almost twice that of the fish AFP, but its S and T contents are significantly greater, indicating much stronger tendency for hydrogen bonding with water or ice. In addition, it has 10 Cs to form five pairs of S=S bridges, enhancing the molecular stability. The unit cell dimensions equivalent to a single protein molecule are $a = 44$ Å, $b = 57$ Å, and $c = 35$ Å. Its globular structure is also shown in Fig. 1. Its molecular weight is 12540 and the scattering length density is 3.50×10^{-6} Å^{-2} in D_2O.

The cfAFP was produced and purified following a process described by Gauthier et al. (20) using a recombinant technology. The protein was grown at 37°C from *Escherichia coli* (BL21-DE3) containing thermal hysteresis protein cDNA in pET20b, and recovered from its inclusion bodies by denaturation and careful refolding. The cfAFP was then oxidized through acidification by addition of sodium acetate, and was then dialyzed. The cfAFP fraction was then purified through both fast protein liquid chromatography and a C18 reverse-phase column. The protein was characterized by the dominant secondary structure of β-sheets.

Experimental procedures for thermal hysteresis measurements

Thermal hysteresis activity is measured by the depression of the freezing temperature from the melting temperature at a given protein concentration. To measure the thermal hysteresis of the effective nucleation temperature, a double oil layer microsized crystallization technique was used (see Liu and Du (28)). This technology allowed us to minimize the influence of the container on ice nucleation, and to examine the ice nucleation kinetics under well-controlled conditions. In brief, a microsized water droplet was suspended in two layers of immiscible oils in a circular quartz cell. A glass coverslip was then placed on the top of the cell to avoid evaporation. Due to the density differences, the water droplet was suspended between the two layers of immiscible oils. To minimize the effect of dust particles, the water and oils were filtered twice using 20-nm filters to remove large particles before they were injected into the cell. The water used in the experiments was in a highly pure deionized form (18.2 MΩ). The ice crystallization was controlled by a Linkam (Surrey, UK) THMS 600 heating and freezing stage, which was capable of controlling the temperature within 0.1°C over the measuring temperature range. Nucleation was observed using a polarized transmitted microscope (BX60-F, Olympus, Tokyo, Japan) to which a 3 charge-coupled device color video camera (KY-F55BE, Osaka, Japan) with an S-VHS video recorder (Panasonic AG-MD830) was attached. Any ice crystal occurring in the drop could immediately be detected by a polarized microscope.

Neutron reflection

Neutron reflectivity, $R(\kappa)$, is defined as the ratio of the intensity of the reflected beam to that of the incoming one and is usually plotted as a function of momentum transfer, κ, perpendicular to the reflecting interface

$$\kappa = \frac{4\pi \sin\theta}{\lambda}, \tag{1}$$

where θ is the incidence angle and λ the wavelength of the incidence neutron beam. Through Fourier transform, $R(\kappa)$ is related to the interfacial composition through the scattering length density perpendicular to the interfacial plane (21,22), $\rho(z)$, by

$$R(\kappa) = \frac{16\pi^2}{\kappa^2}|\hat{\rho}(\kappa)|^2 \tag{2}$$

$$\hat{\rho}(\kappa) = \int_{\infty}^{-\infty} \exp(-i\kappa z)\rho(z)dz, \tag{3}$$

where the scattering length density depends on chemical composition through the following equation:

$$\rho = \sum n_i b_i, \tag{4}$$

where n_i is the number density of the element, i, and b_i is its scattering length. Different isotopes have different b_i values, and isotopic substitution is widely used to highlight the interface. A widely adopted approach is to highlight the adsorbed protein layer using D_2O. The volume fraction of each component within the protein layer is expressed as

$$\rho = \phi_p \rho_p + \phi_w \rho_w, \tag{5}$$

where ρ_p and ρ_w are the scattering length densities of protein and water and ϕ_p and ϕ_w their respective volume fractions. As the protein layer is fully immersed in water at the solid/solution interface, $\phi_p + \phi_w = 1$.

Equations 1–3 outline the principal relationship between $R(\kappa)$ and ρ, but direct Fourier transform is constrained by the narrow κ range within which

the neutron reflectivity profiles are measured. In practice, reflectivity profiles are usually analyzed by means of the optical matrix formalism, which has been described in detail elsewhere (23,24). The structural parameters used in data analysis are the number of layers, thickness (τ), and the corresponding scattering length density (ρ) for each layer (related to layer composition as in Eq. 4). The area per molecule (A) for the protein adsorbed in a uniform layer can be calculated from

$$A = \frac{\sum m_p b_p + n b_w}{\rho \tau}, \quad (6)$$

where $\sum m_p b_p$ is the total scattering length for the protein and n is the number of water molecules associated with each protein molecule. The surface excess can be converted from

$$\Gamma = \frac{MW}{6.02 \times A}, \quad (7)$$

where MW is the molecular weight. In Eq. 7, A is in a unit of Å^2 and Γ is in a unit of mg·m^{-2}. If two or more sublayers are required to describe the nonuniform distribution of the adsorbed protein layer, Eqs. 5–7 are applicable to each sublayer, and the total adsorbed amount is obtained by summing over the sublayers used in the fitting procedure. As stated previously, the choice of the number of sublayers is dependent upon the extent of inhomogeneity across the interface. However, the minimum number of layers that will successfully fit the data is often chosen.

RESULTS AND DISCUSSION

At the onset of the interfacial structural study, solution stability of AFP III was examined by CD and the resulting profile is shown in Fig. 2. For comparison, the CD spectrum taken earlier by Ananthanarayanan et al. (25) from one of the fractions (SP-A) separated from their ion-exchange chromatography is also plotted. Both spectra are similar in shape and they exhibit a broad band around 225 nm and a relatively sharp band near 195 nm, indicating structural similarity. Note that their AFP III was dissolved in 0.1 M NH_4HCO_3 buffer at pH 8 whereas our sample was made in pure water with pH around 7.8. Ananthanarayanan et al. have carefully assessed the effects of temperature and denaturing chemicals on CD spectra and the implications of these factors to structural denaturation. Their studies revealed that well-defined secondary and tertiary protein structures were retained under NH_4HCO_3 buffered aqueous solution. The close similarity between the two curves as shown in Fig. 1 indicates that our AFP III protein sample also retained its native structure in deionized water. The different amplitude around the 195 nm band might arise from minor differences in native protein molecular structure, and experimental conditions such as temperature, solution concentration, and cell path length.

Neutron reflection was first made at the silicon/water interface to characterize the physical structure of the native oxide layer. D_2O was used to highlight the oxide layer so that its thickness and composition were better determined. The measured reflectivity, shown as a dashed line in Fig. 3, was fitted using an optical matrix formula (23,24) and the best fit corresponded to the thickness of 12 Å for the oxide layer. Within the experimental errors, the extent of possible penetration of water into the oxide layer was found to be negligible. No roughness was required to model the measured reflectivity, indicating that the oxide surface was smooth, with the roughness not >3 Å (equivalent to the size of a water molecule).

Subsequent reflectivity measurements were made at the same solid/D_2O interface using fish antifreeze AFP III solution. Fig. 3 shows changes in the reflectivity profiles measured from this protein under a range of concentrations. The reflectivity is mainly detected over the low momentum

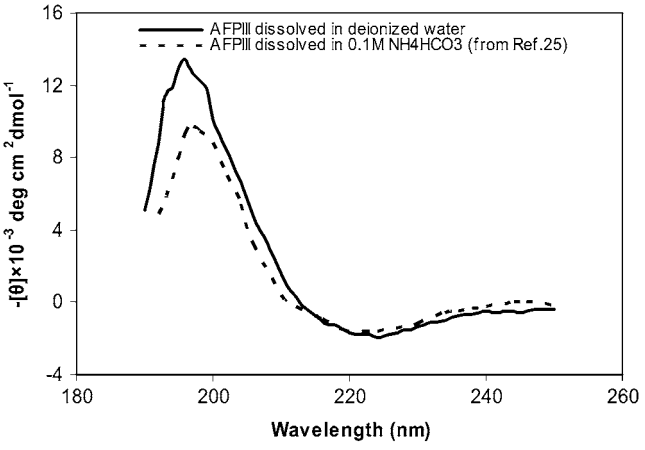

FIGURE 2 CD spectrum obtained from 0.2 mg/ml AFP III at 22°C dissolved in deionized water (*solid line*) is compared with the profile obtained by Ananthanarayanan et al. (25) measured from an AFP fraction separated from ion-exchange chromatography (SP-A) and dissolved in 0.1 M NH_4HCO_3 (pH 8.0) buffer at 0°C. The close similarity in the amplitude and position of the two bands shows that both protein samples retained their native conformations.

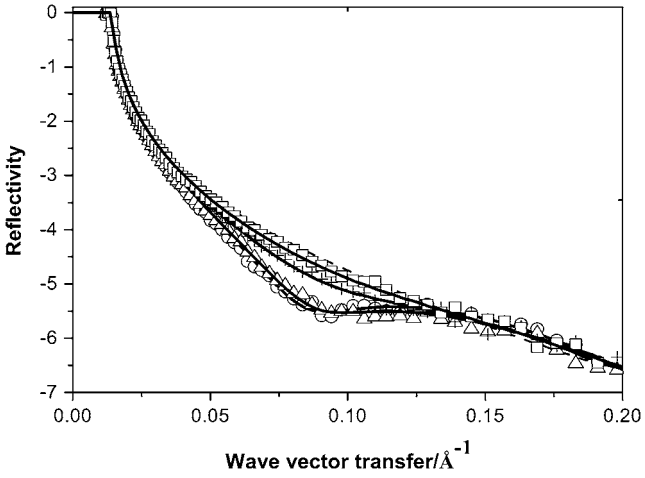

FIGURE 3 Plots of log (neutron reflectivity) measured at the silica/D_2O interface with AFP III (1HZ7) in the solution of 0.01 (□), 0.1 (+), 0.5 (Δ), and 2mg/ml (○). The protein solutions were obtained by directly dissolving AFP lyophilized powder in pure D_2O. The resulted solution pH was generally constant at around pH 7.8. The reflectivity profile from the bare silica/D_2O interface is also given for comparison (*dashed line*). The solid lines are the best fits with parameters given in Table 1.

transfer (κ) region below 0.2 Å^{-1}. At $\kappa > 0.2$ Å^{-1}, it rapidly falls off to the background level. The attainment of constant background and the fast reflectivity decay were indicative of the formation of thin interfacial layers. The reflectivity profiles shown in Fig. 3 had background close to 2×10^{-6}, which has already been subtracted.

It can be seen from Fig. 3 that an increase in protein concentration causes the deviation of the reflectivity from that obtained from the solid/D_2O interface. As the concentration is above 0.5 mg/ml (~0.07 mM), the reflectivity profiles are becoming close to each other, indicating that the adsorption is tending to the saturation.

Information about the thickness and volume fraction of the adsorbed protein layer was obtained by fitting a uniform layer model to the measured data, as outlined previously (23,24). At 1 mg/ml (~0.14 mM), the measured reflectivity was fitted by a thickness (τ) of 32 ± 1 Å and a protein volume fraction of 0.36. Structural parameters under other protein concentrations were obtained similarly and tabulated in Table 1. The thickness derived in the model fitting corresponded to the minimal ψ^2, a residual term indicating the deviation between the measured and calculated data. The main observation from data analysis is that the adsorbed layers could all be fitted in uniform layers with a constant thickness of ~30 Å. It should be noted that below 0.1 mg/ml, the amount of protein adsorbed became low and the reflectivity profiles could be fitted with smaller thicknesses. It was, however, found that the surface adsorbed amount (surface excess) did not vary with different models used. This was well expected because surface excess was proportional to the product of $\tau\rho$, which could still be determined accurately, although the thickness could be less refined.

It is useful to comment that the total scattering length for the protein was calculated from the primary sequence assuming full hydrogen-deuterium exchanges between the labile hydrogens on the protein and D_2O. Some of the labile ones are hindered from the exchange process due to steric encapsulation associated with hydrophobic effect and hydrogen bonding as reported for globular protein structures (26,27). It has been discussed previously that any incomplete exchange would have a small effect on surface excess (well under 5%) but would not undermine the reliability of layer thickness determined (13–15). The crystalline structure for this fish AFP has been resolved by Jia et al. (3,19). Given the small size and the stability of β-sheets in the globular structure, it is well expected that most labile hydrogens would exchange.

TABLE 1 Structural parameters of AFP III (1HZ7) layers with bulk concentration

Conc/mg/ml	τ/Å	($\rho \pm 0.05$) × 10^6/Å^{-2}	$\varphi \pm 0.02$	$\Gamma \pm 0.1$/ mg·m^{-2}	A/Å^2
0.01	32 ± 3	6.00	0.10	0.41	2850 ± 500
0.05	32 ± 2	5.80	0.15	0.61	1910 ± 200
0.1	32 ± 2	5.60	0.21	0.85	1370 ± 150
0.5	32 ± 1	5.10	0.34	1.35	870 ± 80
1.0	32 ± 1	5.05	0.36	1.46	800 ± 50
2.0	32 ± 1	5.00	0.37	1.50	780 ± 50

In parallel, interfacial adsorption of cfAFP (1M8N) from the spruce budworm has also been measured using neutron reflection. Fig. 4 shows the resulting reflectivity profiles after the background subtraction over the same concentration range. As observed previously, protein adsorption caused clear deviation of the reflectivity from that obtained from the SiO_2/D_2O interface. In this case, however, a broad interference fringe was produced around 0.1 Å^{-1}, even at the lowest concentration, indicating a relatively higher adsorption than obtained from the fish AFP III. As the protein concentration increased, the broad interference fringe was shifted to ~0.07 Å^{-1}, indicating the thickening of the layer. As the concentration was increased to 1 mg/ml, the interference fringe was decreased to 0.05 Å^{-1}, with the secondary interference fringe also visible around 0.14 Å^{-1}. Further increase to 2 mg/ml did not cause much change in the shape and position of the reflectivity, indicating the attainment of saturated adsorption.

The same data analysis routine was used to obtain structural parameters from this set of reflectivity profiles. At the two low concentrations, a uniform layer model was appropriate for fitting the measured reflectivity profiles, and the thickness of the layer increased from 30 Å to 45 Å. The corresponding volume fraction increased from 0.28 to 0.32. These changes led to increase in surface excess from 1.2 to 2 mg/m^2. The thickness was close to the two short axial lengths and its increase indicated conformational changes with increasing layer packing density.

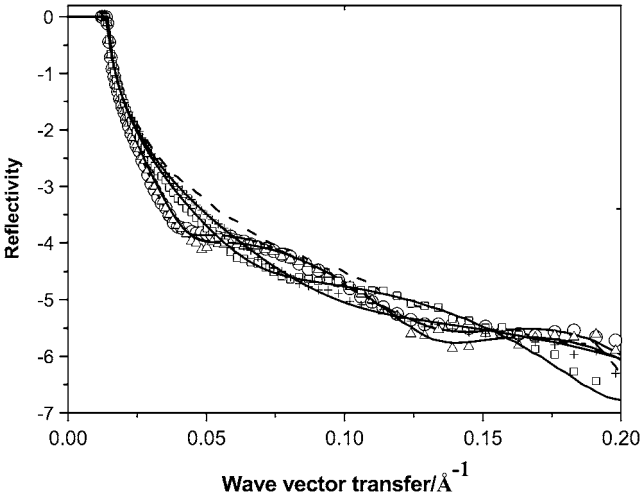

FIGURE 4 Plots of log (neutron reflectivity) measured at the silica/D_2O interface with cfAFP-501 (1M8N) in the solution of 0.01(□), 0.1 (+), 1.0 (Δ), and 2.0mg/mL (○). The protein solutions were obtained by directly dissolving AFP lyophilized powder in pure D_2O. The resulted solution pH was generally constant at around pH 7.8. The reflectivity profile from the bare silica/D_2O interface is also given for comparison (*dashed line*). The solid lines are the best fits with the parameters given in Table 2.

At the two high concentrations, it was found that uniform layer model did not produce adequate fit to the measured reflectivity profiles at all. Neither did the two-layer models. The least number of sublayers required to fit the measured profiles was three. Table 2 lists the thickness, the scattering length, and volume fraction for each sublayer together with the corresponding surface excess. It can be seen that the main part of the protein stays within the middle sublayer; the inner and outer sublayers contain a minor amount only. This structural feature may suggest that the protein adopts a range of conformational orientations at the interface. If the protein adsorbs with its ice-binding plane on the surface of SiO_2 in the same manner as described when binding at the ice/water interface, the thickness of the layer would be close to the two short axes around 40 Å. The thickness of the middle sublayer is where most protein stays and is greater than this dimension, indicating that the average protein molecule is rather tilted. It has been reported that 1M8N has other faces that can also initiate ice binding and self-associate within the interface (6,8,20). This structural characteristic is highly related to the observed structural progression at the SiO_2/water interface and is distinctly different from the adsorption observed from the fish AFP. Different faces on the protein molecule may have different structural requirement and energetic barriers, which are consistent with the structural transition observed from the protein layers.

The variations of surface excess as a function of bulk concentration for both AFP proteins are listed in Tables 1 and 2, where it can be seen that the adsorption of fish AFP tends to plateau, resembling a Langmuir type of isotherm. In contrast, the trend for the insect AFP over the same concentration range shows further increase, but tends to plateau more slowly, indicating possible multilayer formation. The insect cfAFP surface excess is consistently higher over the entire concentration range studied. Over the low concentration range, the surface excess from the insect cfAFP is twice that obtained from the fish AFP III, but as the concentration increases the difference becomes even greater.

The Langmuir isotherm can be written as

$$\theta = \frac{KC}{1 + KC}, \tag{8}$$

where K is the adsorption constant, C is the protein concentration, and θ is the fraction of surface coverage and is equal to Γ/Γ_∞, where Γ_∞ is the saturation surface excess. Equation 8 can be subsequently converted into

$$\frac{1}{\Gamma} = \frac{1}{\Gamma_\infty} + \frac{1}{K\Gamma_\infty C}. \tag{9}$$

The plot of $1/\Gamma$ against $1/C$ should be a straight line if the experimental data follow the Langmuir isotherm. The experimental results, as plotted in Fig. 5, show that neither of the protein adsorption profiles follows the ideal Langmuir type of behavior over the entire concentration range studied. In fact, it can be seen from Fig. 5 that the two curves are rather similar in shape, indicating similar concentration-dependent physicochemical characteristics. The deviation from the Langmuir isotherm is perhaps not surprising in light of the high surface packing density and extensive structural changes (particularly in case of the insect protein) as revealed by neutron reflection.

In an effort to correlate the observed surface excess difference to antifreeze performance, we have measured the thermal hysteresis of the two antifreeze proteins using the methodology already established previously (28). Fig. 6 shows that as the concentration of the fish antifreeze increases its suppression on the ice freezing, consistent with the trend of surface excess obtained. Although the parallel thermal hysteresis study for the insect antifreeze was made at 0.5 mg/ml only due to the lack of sufficient sample, the result is sufficiently reliable to indicate a much stronger suppression of the ice freezing point, again consistent with the observed greater surface excess from the insect protein. The effects of ice crystal growth inhibition for both AFPs have also been compared by Tyshenko et al. (10). They showed that with increasing concentration, the thermal hysteresis increased for both proteins, but at the concentration above 1 mg/ml, the insect cfAFP was several times more effective. Note that the insect cfAFP used in their work had a smaller molecular weight and was inherently less effective than isoform 501 used in this study. Leinala et al. (9) have examined the inhibition effects from cfAFP-501 and its smaller isoform cfAFP-337. Strong inhibition to ice crystal growth was observed from both isoforms below 0.1 mM. CfAFP-501 produced the stronger effect overall, but it showed a sharp concentration dependent effect below 0.05 mM, the same concentration range where a drastic variation in structure and

TABLE 2 Structural parameters of cfAFP-501(1M8N) layers with bulk concentration

Conc (mg/ml)	τ/Å	$(\rho \pm 0.05) \times 10^{-6}$/Å^{-2}	$\varphi \pm 0.01$	$\Gamma \pm 0.1$/mg·m^{-2}	Γ_{total}/mg·m^{-2}	A/Å^2
0.01	$\tau_1 = 30 \pm 2$	$\rho_1 = 5.54$	0.28	1.18	1.18 ± 0.15	1765 ± 180
0.1	$\tau_1 = 45 \pm 2$	$\rho_1 = 5.45$	0.32	2.03	2.03 ± 0.15	1025 ± 100
1.0	$\tau_1 = 5 \pm 2$	$\rho_1 = 5.65$	0.25	0.18	4.18 ± 0.3	500 ± 40
	$\tau_2 = 61 \pm 1$	$\rho_2 = 5.10$	0.44	3.78		
	$\tau_3 = 22 \pm 3$	$\rho_3 = 6.15$	0.07	0.22		
2.0	$\tau_1 = 6 \pm 2$	$\rho_1 = 6.10$	0.09	0.08	4.82 ± 0.3	430 ± 40
	$\tau_2 = 62 \pm 1$	$\rho_2 = 4.95$	0.49	4.29		
	$\tau_3 = 26 \pm 3$	$\rho_3 = 6.00$	0.12	0.45		

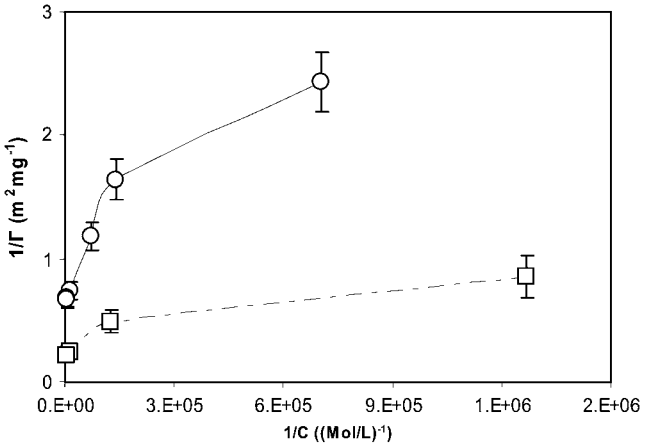

FIGURE 5 Plots of 1/Γ (surface excess) versus 1/C (bulk concentration) for fish AFP III (○) and insect cfAFP-501 (□). The lines were drawn to guide the eye.

composition of the adsorbed layer was observed in our work. It can thus be said that although the current adsorption measurement was made at the SiO_2/water interface, remarkable correlation has been obtained between protein adsorption and the changing activity in thermal hysteresis for both AFPs. Thus differences in the adsorbed amount and layer structure correlate well with the reported difference in thermal hysteresis between them, directly relating to the extent of inhibition to ice crystal growth.

It is widely recognized that the power of inhibition of ice crystal growth originates from the presence of a flat surface on the protein molecule that structurally matches the ice lattice (11,12). The adsorption of protein molecules breaks the lattice structure and limits ice growth. Although our experiment has no structural resolution to the ice-binding lattice surface, the surface excess obtained shows a strong correlation to the inhibition of ice crystal growth for both AFP proteins. The neutron data show that the fish AFP adsorbs with broadly the same orientation at the interface. Increase in bulk concentration increases surface coverage only. Assuming that the footprint of the adsorbed protein is equivalent to the product of the two large axes, the area is equal to 1755 $Å^2$. The fraction of the surface area occupied is 0.62 and 0.92 at the two lowest concentrations of 0.01 and 0.05 mg/ml, respectively, indicating the presence of some empty gaps between protein molecules at the interface. With increasing protein concentration and surface excess, the actual area occupied per protein molecule was smaller than the limiting area of 1755 $Å^2$ estimated, showing a clear trend of increasing surface packing and possible structural deformation with bulk protein concentration. The high packing density is associated with the structural flexibility of the fish AFP molecules. The high surface coverage provided high inhibition to ice crystal growth.

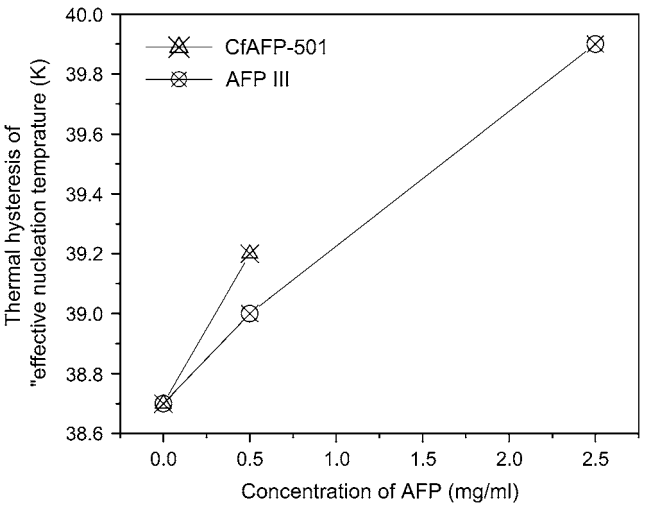

FIGURE 6 Thermal hysteresis measured against fish AFP III and insect cfAFP concentrations.

Note that the vast packing density changes for fish AFP III occurred without any alteration to the layer thickness. Comparatively, the insect cfAFP showed steady changes in both interfacial structure and packing density. Over the high protein concentration range, the volume fraction of protein within the interfacial layer was below 0.4 for the fish AFP and was below 0.5 for the insect cfAFP within the densely packed middle sublayer. These were much lower than the values of 0.6–0.7 as observed from lysozyme and bovine serum albumin from the same interface (13–16). It would thus seem that although AFPs are very effective at inhibiting ice crystal growth via interfacial adsorption, their interfacial packing densities are actually lower than most other proteins we have recently characterized.

Fig. 7 depicts the schematic representation of the characteristic structural features of the protein layers observed from neutron reflection. The adsorption of fish AFP III forms a uniform protein layer with the thickness around 32 Å, close to the height of the globular molecule if it is assumed that its ice-binding surface sits on the SiO_2 surface. Decrease in protein concentration reduces the surface coverage over the concentration range studied, broadly consistent with the reported reduction in the inhibition of ice crystal growth (7). For the insect protein cfAFP, the amount of adsorption over the same concentration range is persistently higher and the structure of the adsorbed layer shows a steady variation with increasing surface excess. The initial increase in surface packing density appears to cause the molecule to alter the face in contact with the SiO_2 surface. Subsequent concentration increase leads to a range of conformational orientations as a result of binding and interaction within the interfacial layer. The more flexible response of the insect protein to the increased surface packing density might be directly responsible for its more effective inhibition of ice crystal growth.

The lateral interaction associated with in-plane oligomerization has been thought to be important in the action of AFPs in their interfacial adsorption. Deluca et al. have tried to

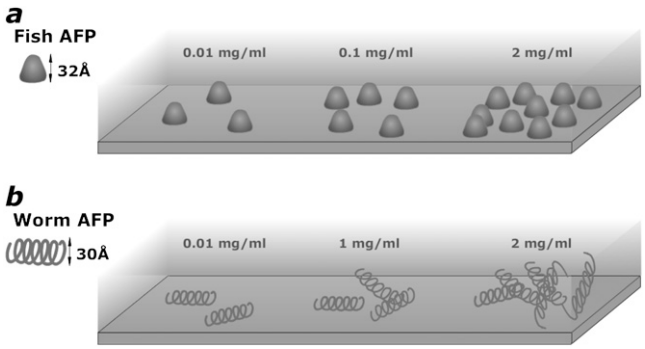

FIGURE 7 Schematic representation of the adsorption from fish AFP III (1GH7) (*a*) and insect cfAFP (1M8N) (*b*) in a concentration-dependent manner.

examine this effect by linking thioredoxin and maltose-binding protein onto AFPs to prevent lateral oligomerization (12), but surprisingly they found an increased antifreeze activity over the wild-type of fish AFP III. In light of our study, we believe that the observed enhancement in antifreeze activity from the modified ones was possibly due to the increased adsorption.

In addition to the possible difference between the ice surface and hydrated SiO_2, the above study was made at the ambient temperature of 23°C. Graether et al. have recently showed some small but measurable temperature effect on the structure of insect cfAFP, particularly to the folds at the N-terminal (29). They have also shown that above 2 mM, oligomerization such as dimer or trimer formation might be important at the ambient temperature in cfAFP solution. The neutron reflection work has, for the first time, demonstrated that the affinity between cfAFP molecules was an important factor to cause the observed structural changes at the interface. Note that the concentrations studied were below 2 mM, but the interfacial oligomerization might occur at the concentration well below that required in the bulk solution. The structural features as revealed at the high AFP concentration range studied were associated with the formation of oligomers.

CONCLUSIONS

Extensive research by x-ray crystallography and NMR has been undertaken to determine the structures of different antifreeze proteins, with the aim of identifying the protein surfaces that are capable of binding to ice. Less pursued has been to characterize the adsorption properties of these AFP proteins because direct study of this process at the ice/water interface is technically difficult. We show in this work that using hydrophilic silicon oxide as substrate AFP adsorption can be facilitated by neutron reflection, a technique that has been used for studying adsorption of other proteins and synthetic polymers. To our knowledge, this is the first time that neutron reflection has been used to determine the structural features of adsorbed AFP layers. The main finding from neutron reflection is that the data obtained are broadly consistent with the different thermal hysteresis and ice-inhibiting effects reported for the two AFP proteins, and therefore are meaningful. Given that the SiO_2 surface is very likely to be different from the crystalline structure of ice surface, the neutron work reported here suggests that the general adsorption properties of these AFPs need to be characterized. This area of study will contribute to the current pursuit of the structural complementarity between the ice surface and the ice-binding face of the proteins.

The neutron data show that the fish AFP III adsorption formed a uniform layer with its ice-binding face in contact with the substrate surface. Change in bulk concentration did not appear to affect the layer thickness but the surface coverage. The surface excess tended to plateau, but did not follow the Langmuir isotherm, suggesting a changing in-plane interaction associated with the large variation in layer packing density. In contrast, the insect cfAFP protein produced a steady change of layer structure as well as packing density, consistent with the presence of several faces for ice-binding and intermolecular recognition within the surface plane. At low surface excesses, the protein appeared to use its large faces in direct contact with the substrate surface. As the surface excess increased, the lateral repulsion increased and the conformational orientation was switched such that its different ice-binding face was in direct contact with SiO_2 and the surface adsorbed amount could be maximized. The changing surface structure with concentration was accompanied by the steady rising surface adsorbed amount and much more effective ability to inhibit ice growth.

We thank the Biotechnology and Biological Sciences Research Council, the Engineering and Physical Sciences Research Council for financial support, and the ISIS Neutron Facility for providing neutron beam time. X.Z. thanks Biocompatibles UK Ltd. and S.P. thanks the ISIS Neutron Facility for studentships.

REFERENCES

1. Ewart, K. V., Q. Lin, and C. L. Hew. 1999. Structure, function and evolution of antifreeze proteins. *Cell. Mol. Life Sci.* 55:271–283.
2. Fletcher, G. L., C. L. Hew, and P. L. Davies. 2001. Antifreeze proteins of teleost fishes. *Annu. Rev. Physiol.* 63:359–390.
3. Antson, A. A., D. J. Smith, D. I. Roper, S. Lewis, L. S. Caves, C. S. Verma, S. L. Buckley, P. J. Lillford, and R. E. Hubbard. 2001. Understanding the mechanism of ice binding by type III antifreeze proteins. *J. Mol. Biol.* 305:875–889.
4. Sicheri, F., and D. S. C. Yang. 1995. Ice binding structure and mechanism of an antifreeze protein from winter flounder. *Nature*. 375:427–431.
5. Duman, J. G. 2001. Antifreeze and ice nucleator proteins in terrestrial arthropods. *Annu. Rev. Physiol.* 63:327–357.
6. Graether, S. P., and B. D. Sykes. 2004. Cold survival in freeze-intolerant insects the structure and function of β-helical antifreeze proteins. *Eur. J. Biochem.* 271:3285–3296.
7. Raymond, J. A., and A. L. Devries. 1977. Adsorption inhibition as a mechanism of freezing resistance in polar fishes. *Proc. Natl. Acad. Sci. USA.* 74:2589–2593.

8. Doucet, D., M. G. Tyshenko, P. L. Davies, and V. K. Walker. 2002. A family of expressed antifreeze protein genes from the moth, *Choristoneura fumiferana*. *Eur. J. Biochem.* 269:38–46.

9. Leinala, E. K., P. L. Davies, D. Doucet, M. G. Tyshenko, V. K. Walker, and Z. Jia. 2002. A β-helical antifreeze protein isoform with increased activity structural and functional insights. *J. Biol. Chem.* 277:33349–33353.

10. Tyshenko, M. G., D. Doucet, P. L. Davies, and V. K. Walker. 1997. The antifreeze potential of the spruce budworm thermal hysteresis protein. *Nat. Biotechnol.* 15:887–890.

11. Leinala, E. K., P. L. Devies, and Z. Jia. 2002. Crystal structure of β-helical antifreeze protein points to a general ice binding model. *Structure*. 10:619–627.

12. Deluca, C. I., R. Comley, and P. L. Davies. 1998. Antifreeze proteins bind independently to ice. *Biophys. J.* 74:1502–1508.

13. Su, T. J., J. R. Lu, R. K. Thomas, Z. F. Cui, and J. Penfold. 1998. The effect of pH on the adsorption of lysozyme at the hydrophilic silicon oxide-water interface, a neutron reflection study. *Langmuir*. 14: 438–445.

14. Su, T. J., J. R. Lu, R. K. Thomas, Z. F. Cui, and J. Penfold. 1998. The adsorption of lysozyme at the silica-water interface: a neutron reflection study. *J. Colloid Interface Sci*. 203:419–429.

15. Su, T. J., J. R. Lu, R. K. Thomas, Z. F. Cui, and J. Penfold. 1998. The conformational structure of bovine serum albumin layers adsorbed at the silica-water interface. *J. Phys. Chem. B*. 102:8100–8108.

16. Lu, J. R., T. J. Su, R. K. Thomas, and J. Penfold. 1998. Binding of surfactants onto pre-adsorbed layers of bovine serum albumin at the silica-water interface. *J. Phys. Chem. B*. 102:10307–10315.

17. Lu, J. R., T. J. Su, R. K. Thomas, and J. Penfold. 1998. Binding of sodium dodecyl sulphate to bovine serum albumin layers adsorbed at the silica-water interface. *Langmuir*. 14:6261–6268.

18. Fragneto, G., J. R. Lu, D. C. McDermott, R. K. Thomas, P. D. Gallagher, and S. K. Satija. 1996. Structure of monolayers of tetraethylene glycol monododecyl ether adsorbed on self-assembled monolayers on silicon: a neutron reflectivity study. *Langmuir*. 12:477–486.

19. Jia, Z., C. I. DeLuca, H. Chao, and P. L. Devies. 1996. Structural basis for the binding of a globular antifreeze protein to ice. *Nature*. 384: 285–288.

20. Gauthier, S. Y., C. M. Kay, B. D. Sykes, V. K. Walker, and P. L. Davies. 1998. Disulfide bond mapping and structural characterization of spruce budworm antifreeze protein. *Eur. J. Biochem.* 258:445–453.

21. Lu, J. R., E. M. Lee, and R. K. Thomas. 1996. The analysis and interpretation of specular neutron and x-ray reflection. *Acta Crystallogr. A*. 52:11–41.

22. Lu, J. R., and R. K. Thomas. 1998. Neutron reflection from wet interfaces. *J. Chem. Soc., Faraday Trans*. 94:995–1018.

23. Born, M., and E. Wolf. 1970. Principles of Optics. Pergamon, Oxford, UK.

24. Lekner, J. 1987. Theory of Reflection. Nijhoff, Dordrecht, The Netherlands.

25. Ananthanarayanan, V. S., D. Slaughter, and C. L. Hew. 1986. Antifreeze proteins from the ocean pout, *Macrozoarces americanus*: circular dichroism spectral studies on the native and denatured states. *Biochim. Biophys. Acta*. 870:154–159.

26. Radford, S. E., K. D. Buck, K. D. Topping, C. M. Dobson, and P. A. Evans. 1992. Hydrogen exchange in native and denatured states of hen egg-white lysozyme. *Proteins Struct. Funct. Genet.* 14:237–248.

27. Hvidt, A., and S. O. Nielsen. 1966. Hydrogen exchange in proteins. *Adv. Protein Chem.* 21:287–386.

28. Liu, X. Y., and N. Du. 2004. Zero sized effect of nanoparticles and inverse homogeneous nucleation principles of freeze and antifreeze. *J. Biol. Chem.* 279:6124–6131.

29. Graether, S. P., S. M. Gragne, G. L. Spyracopouloos, Z. Jia, P. L. Davies, and B. D. Sykes. 2003. Spruce budworm antifreeze protein: changes in structure and dynamics at low temperatures. *J. Mol. Biol.* 327:1155–1168.